Quantum charge pumping and electric polarization in Anderson insulators

Chyh-Hong Chern*

Institute for Solid State Physics, University of Tokyo, Kashiwanoha 5-1-5, Kashiwa 277-8581, Japan

Shigeki Onoda and Shuichi Murakami

CREST, Department of Applied Physics, University of Tokyo, 7-3-1 Hongo, Tokyo 113-8656, Japan

Naoto Nagaosa

CREST, Department of Applied Physics, University of Tokyo, 7-3-1 Hongo, Tokyo 113-8656, Japan
and Correlated Electron Research Center, National Institute of Advanced Industrial Science and Technology, 1-1-1 Higashi, Tsukuba,
Ibaraki 305-8562, Japan

We investigate adiabatic charge pumping in the disordered system in one dimension with open and closed boundary conditions. In contrast to the Thouless charge pumping, the system has no gap even though all the states are localized, i.e., strong localization. Charge pumping can be achieved by making a loop adiabatically in the two-dimensional parameter space of the Hamiltonian. It is because there are many δ-function-like fluxes distributed over the parameter space with random strength, in sharp contrast to the single δ-function in the pure case. This provides a more efficient way of charge pumping and polarization.

I. INTRODUCTION

The quantum dynamics of the charge in insulators is a rich and nontrivial issue. In the dc limit, the conductivity vanishes, but it does not imply that the charge motion is frozen in the insulators. One example is the ferroelectricity and electric polarization in the insulators. The classical definition of the electric polarization $\vec{P} = \int d\vec{r}\,\vec{r}\rho(\vec{r})$ [$\rho(\vec{r})$: charge density] fails for the extended Bloch wave functions since the $\vec{r}$ is unbounded. This difficulty is avoided by considering instead the different definition for the *difference* of the polarization,[1–5]

$$\Delta\vec{P} = \int_0^T d\tau \frac{d\vec{P}}{d\tau},\tag{1}$$

where the change of the polarization between the initial and final states is given by the integral of the polarization *current* during the adiabatic change of the parameters $\vec{Q} = (Q_1, Q_2, \ldots, Q_n)$ such as the atomic displacements. One can usually choose the initial state with the inversion symmetry without electric polarization, and Eq. (1) determines the polarization of the final state of our interest. Here, by using $\frac{d\vec{P}}{d\tau} = \frac{d\vec{P}}{dQ_i}\frac{dQ_i}{d\tau}$, the μ component of $\Delta\vec{P}$ is expressed as

$$\Delta P_\mu = \int_C d\vec{Q} \cdot \frac{dP_\mu}{d\vec{Q}},\tag{2}$$

with the path C specified by $\vec{Q} = \vec{Q}(\tau)$. What is found by Resta[3] and King-Smith and Vanderbilt[4] is that $\frac{dP_\mu}{d\vec{Q}}$ can be represented by the Berry phase, which fits to the first-principles band calculation. Then, the question arises: "Is there any path (C) dependence of the polarization?" It is clear that there is no parametrization dependence since we consider the adiabatic change, but the different paths C_1 and C_2 in the $\vec{Q}$ space might lead to the different values of $\Delta\vec{P}$. This is related to the single valueness and the Chern number of the Bloch wave function. Onoda and co-workers addressed this problem as follows by analyzing the one-dimensional two-band models characterized by the three-dimensional $\vec{Q}$.[6,7] There appears a singular line, i.e., a string, in the $\vec{Q}$ space corresponding to the trajectory of the monopole (band-crossing point) as the momentum k moves, which acts as the "current circuit" to produce the "magnetic field" $\frac{dP}{d\vec{Q}}$ via the Biot-Savart law. Away from the string, the system is always gapped and insulating. When the adiabatic change of the parameter $\vec{Q}$ makes a loop enclosing the string, the charge is pumped during this process, which is quantized to be an integer multiple of e since the strength of the current is quantized. This is a realization of the quantum charge pumping proposed by Thouless.[8] The analogy to the magnetostatics says that the polarization is path independent as long as the loop $C = C_1 + (-C_2)$ does not enclose the string. This is usually the case because the change of the parameter $\vec{Q}$ is rather small and we need the huge variation of $\vec{Q}$ to enclose the string, i.e., gapless states. In other words, the ferroelectricity can be regarded as "a fraction of the quantum charge pumping."

This type of charge pumping can be regarded as the rigid shift of the wave function due to the change in the external parameters such as the atomic positions. It is natural when the wave function consists of the Bloch states extending over the whole sample, and then the quantum interference pattern is modified by the external parameters. One can estimate roughly how much the charge is pumped as below. Let the dimension of the parameters be the energy. Then, the distance between the physically realized set of parameters and that of gapless states, i.e., string, is the energy gap E_G. Let Δ be the change of the parameters in units of energy. The angle subtended by this *segment* in parameter space is roughly es-

timated as $2\pi\Delta/E_G$. Since the 2π winding corresponds to unit charge e shifting by one lattice constant a, i.e., $P_0=ea$, the polarization is roughly given by $P=ea\Delta/E_G$.[6] Therefore, to enhance the dielectric response, one can reduce E_G or enlarge Δ. A possible method to reduce E_G is to introduce a substrate disorder, by which even the gapless insulator can be realized. However, the electron wave functions are no longer the extended Bloch states in the presence of the disorder, and one needs to worry about the localization, i.e., the Anderson localization. When all the states are strongly localized, one cannot transmit the phase information through the sample and hence cannot expect the charge pumping either. On the other hand, as emphasized, the charge pumping is closely related to the topological nature of the wave functions in the parameter space, which is robust against the disorder to some degree. For example, in the two-dimensional electron systems under the strong magnetic field, there occur discrete extended states *protected by the topology*. Namely, the Chern number is carried by the extended states only, which is not destroyed by the weak disorder. Nevertheless, a similar situation arises even in the one-dimensional systems, which will be extensively studied in the following sections. Niu and Thouless[9] studied the stability of the charge pumping against the weak disorder by a topological argument. Even though all the states are localized, the charge pumping was shown to be unchanged as long as the gap remains finite. However, questions still remain, such as what is the physical mechanism of the charge pumping through the localized states and what happens when the gap collapses.

In this paper, we study the effect of the disorder on the charge pumping and dielectric response in a one-dimensional model for the insulators. Combining the numerical simulation and analytic considerations, we reveal the physical picture of the charge pumping by the localized states both in the case of the open boundary condition and the periodic/twisted boundary condition. The former one is more relevant to the experimental situation such as the ferroelectric random access memory (FeRAM) where the leads are attached to the thin film of the insulators, while the latter is more appropriate to see the role of topology. We have published a Letter summarizing the results on the open boundary condition.[10] This paper provides the full details of the formulation, calculations, and the additional results on the open system, as well as results on the periodic/twisted boundary condition.

The plan of this paper is as follows. In Sec. II, a model for the disordered insulator showing the charge pumping is introduced. Its analysis with the open boundary condition is given in Sec. III, including a detailed description of the resonant tunneling mechanism. In Sec. IV, we analyze the model by using the three-dimensional parameter space, including the phase angle α for the twisted boundary condition, and introduce the role of the magnetic monopoles in this space. Section V is devoted to the conclusions.

II. MODEL FOR A DISORDERED INSULATOR

The minimal model for ferroelectrics is given by the following ionic dimer model:
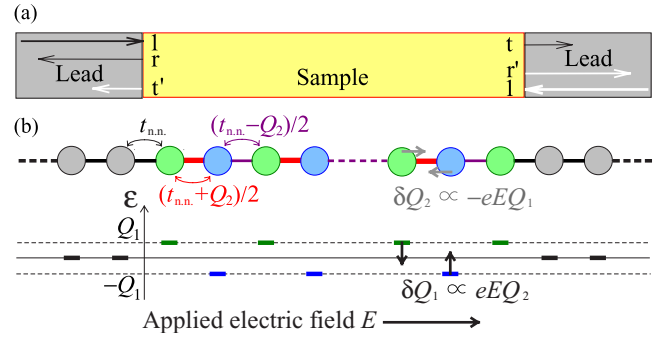
(a)

(b)

FIG. 1. (Color online) Ionic dimer system sandwiched by the leads.

$$H_{\mathrm{pure}} = -\frac{1}{2}\sum_{i=1}^{L}[t_{\mathrm{nn}} - (-)^i Q_2](c_{i+1}^\dagger c_i + \mathrm{H.c.}) + \sum_{i=1}^{L}(-)^i Q_1 c_i^\dagger c_i. \tag{3}$$

Here, c_i and $c_i^\dagger$ are the annihilation and creation operators of the electron at the site $i=1,\ldots,L$, where L is the number of sites. For the open system attached to the leads, c_{L+1} and $c_{L+1}^\dagger$ represents the operators in one of the leads, while for the closed system, they are understood as c_1 and $c_1^\dagger$. t_{nn} is the transfer integral. Q_1 and Q_2 represent the alternations of the local ionic level and the bond dimerization, respectively. The spin degree of freedom is omitted for simplicity. We consider the half-filling case which is the most relevant to the ferroelectrics. Although this model might look special, it illustrates the two essential features of the ferroelectrics, i.e., (i) the two species of the ions characterized by the level alternation Q_1 and (ii) the relative shift of the atomic positions described by the dimerization Q_2. Therefore, it is able to describe the ferroelectricity in BaTiO$_3$, where Ti and O are dimerized to produce the polarization.[11] It can be also applied to the quasi-one-dimensional ferroelectric materials such as organic charge transfer compounds TTF-chloranil[12] and (TMTTF)$_2 X$ (X=PF$_6$, AsF$_6$, S$_6$F$_6$, SCN).[13]

The Hamiltonian H_{pure} with the periodic boundary condition has two bands,[6]

$$\varepsilon_{\pm}(k) = \pm\sqrt{t_{\mathrm{nn}}^2\cos^2 k + Q_1^2 + Q_2^2\sin^2 k}. \tag{4}$$

Experimentally, the parameters $\vec{Q}\equiv(Q_1,Q_2)$ can be controlled by applying the electric field E along the polarization direction and the pressure p. The procedure may go as follows: Electrons at high and low deinsity sites shift relatively in the opposite directions, as shown in open arrows of Fig. 1(b). Change the dimerization Q_2 by $\delta Q_2 \propto eEQ_1$. Simultaneously, within each dimer, a level difference Q_1 changes by $\delta Q_1 \propto -eEQ_2$, as illustrated by black arrows in Fig. 1(b). Therefore, the electric field E mainly controls the angle

$$\theta = \arctan(Q_2/Q_1). \tag{5}$$

Applying the pressure, one can increase the hybridization and reduce the ratio Q/t_{nn} with
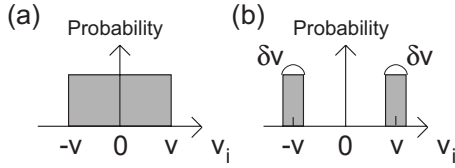
$$Q = \sqrt{Q_1^2 + Q_2^2}. \tag{6}$$

FIG. 2. (a) Uniform distribution of the on-site random potential. (b) Alloy model for the on-site random potential, which mimics effects of substitution in alloys.

To discuss the quantum relaxor behavior, we introduce the on-site random potential v_i to the Hamiltonian given by Eq. (3),

$$H = H_{pure} + \sum_{i=1}^{L} v_i c_i^\dagger c_i. \qquad (7)$$

The type of the random distribution takes either a uniform distribution or an alloy model, which are shown in Fig. 2. In the following, we study effects of an on-site disorder on dielectric properties in both open and closed systems, particularly focusing on the topological aspects.

III. OPEN BOUNDARY CONDITION

In this section, we solve Eq. (3) numerically with two different situations: a single-channel problem with a uniformly distributed random potential and a multichannel problem in an alloy model for an on-site random potential. The latter corresponds to the realistic situation in the FeRAM devices, where the polarization is measured by the integrated current flowing in the leads. When the size of the sample becomes nanoscale, the quantum nature of the polarization is expected to play essential roles via an unusual quantum interference.[6,8] Namely, the quantum coherence is maintained throughout the sample. From the application point of view, it is required to achieve (i) a magnitude of the polarization larger than 10 μC/cm^2, (ii) a leak current smaller than $0.1-1$ μA/cm^2, and (iii) a dielectric constant larger than 300.[14] By introducing a disorder, one can suppress the dissipation from the leak current because of the strong localization effect.[9,15] In addition, the reduction of the energy gap takes place to enhance the dielectric properties. Actually, a similar idea has been realized in the relaxor ferroelectrics[16–18] and the pinned charge-density-wave systems,[19] though their mechanism is due to a classical mesoscopic cluster formation analogous to spin glass systems.

In the strong disordered case, the charge transfer can occur due to the resonant tunneling, which has an interesting counterpart for the adiabatic charge pumping through the quantum dot.[20] Theoretically, it is possible to achieve as the control parameters are chosen to be the function of the sample size and disorder strength.[21–23] Here, we propose the possibility of the enhancement of the dielectric response in the insulators by a disorder in nanoscopic/mesoscopic multichannel systems and estimate the operational time for the dissipationless adiabatic charge displacement. The application to the memory devices, for example, FeRAM,[14] shall be also discussed.

A. Single-channel problem for a uniformly distributed random potential

Let us consider an insulating electronic system sandwiched by two leads (electrodes), as shown in Fig. 1(a). For simplicity, we take a one-dimensional (single-channel) model, but the extension to higher dimensional (multichannel) cases is straightforward, as discussed in the later section.

We take the total Hamiltonian

$$H_{tot} = H + H_{lead}, \qquad (8)$$

where H and H_{lead} are given by Eq. (7) and

$$H_{lead} = -\frac{t_{nn}}{2} \left(\sum_{i=0}^{-\infty} + \sum_{i=L}^{\infty} \right)(c_{i+1}^\dagger c_i + \text{H.c.}), \qquad (9)$$

respectively. This model is schematically shown in Fig. 1(b). The Green's function $G_{i,i'}(\varepsilon)$ for the above model is readily obtained from the recursion formula in the form of the continued fraction.[24] Here, we concentrate on the case where the chemical potential is located at the zero energy.

We adopt the Landauer-Büttiker formalism,[24,25] where the sample is regarded as a *scatterer* characterized by the scattering S matrix

$$S = \begin{pmatrix} r & t \\ t' & r' \end{pmatrix}, \qquad (10)$$

where r and r' are the reflection coefficients and t and t' are the transmission coefficient (see Fig. 1) The transmittance through the sample and the reflectance for both ends satisfy the following unitary relations:

$$T = |t|^2, \qquad (11)$$

$$R = |r|^2 = 1 - T, \qquad (12)$$

$$T' = |t'|^2, \qquad (13)$$

$$R' = |r'|^2 = 1 - T', \qquad (14)$$

$$r^* t' + r' t^* = 0. \qquad (15)$$

In the steady state, $T = T'$ and $R = R'$. Then, we employ Brouwer's formula,[26,27] which is originally discussed in quantum dot systems. The pumping charge Δq from the left to the right through the adiabatic change of parameters $\vec{Q}$ along a path C is given by[26]

$$\Delta q = e \int_C \frac{d\vec{Q}}{2\pi} \cdot \text{Im}(r^* \vec{\nabla}_Q r + t \vec{\nabla}_Q t^*). \qquad (16)$$

Therefore, even in the perfectly reflecting case where $t = 0$ and $|r| = 1$, the charge can be pumped by controlling the phase φ of $r = e^{i\varphi}$.[28]

Let us start with the pure case ($v_i = 0$). Without the random potential v_i, the bulk system has an energy gap

$$E_{G0} = 2\sqrt{Q_1^2 + \text{Min}\{t_{nn}^2, Q_2^2\}}. \qquad (17)$$

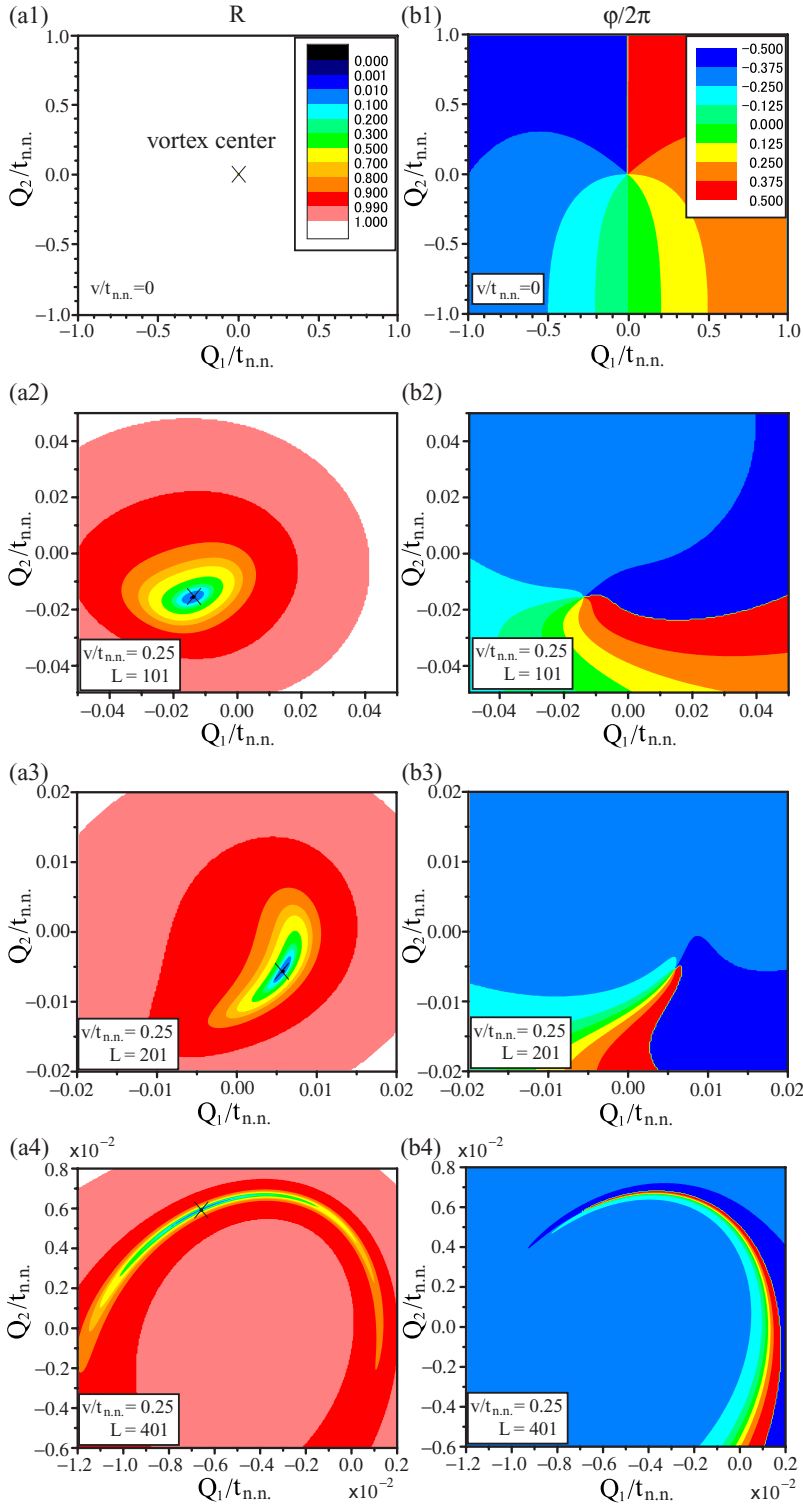This gap closes at $\vec{Q} = \vec{0}$, where the finite conduction occurs.

FIG. 3. (Color online) Reflectance $R=|r|^2$ and the phase $\varphi=\arg r$. [(a1) and (b1)] Clean bulk system. [(a2) and (b2)] Disordered system of finite size $L=401$ with the random potential of the strength $v/t_{nn}=0.5$. The color code given in (a1)/(b1) also applies to (a2),(a3)/(b2),(b3). In the white region in (a1)–(a3), R is the unity within the accuracy of 10^{-4}.

This defines the vortex center of the reflective coefficients r and r'. By means of the continued-fraction expansion of the Green's function, the analytic form of r in the thermodynamic limit $L\rightarrow\infty$ is obtained as

$$r=-\frac{Q_1^2+t_{nn}Q_2+Q\sqrt{t_{nn}^2+Q_1^2}+2it_{nn}Q_1}{Q_1^2+t_{nn}Q_2+Q\sqrt{t_{nn}^2+Q_1^2}-2it_{nn}Q_1}, \qquad (18)$$

where $Q\equiv\sqrt{Q_1^2+Q_2^2}$. The panels (a1) and (b1) of Fig. 3 show

the reflectivity $R=|r|^2$ for $L=10\,001$ and the phase φ of r for $L\rightarrow\infty$ without disorder. The phase winds by 2π around $\vec{Q}=(0,0)$ and the "vortex core" can be clearly seen representing $r=0$ and $|t|=1$. In the thermodynamic limit $L\rightarrow\infty$, $R=1$ and $T=0$ hold, except at the vortex core. For the finite-size systems, the transmittance T behaves as e^{-L/ξ_0}, with $\xi_0=t_{nn}/E_{G0}$. Therefore, the size of the region in the $\vec{Q}$ space with a large T is of the order of t_{nn}/L for a large L. In other

words, the vortex is the gapless point and leads to the perfect transmittance.

Remarkably, this perfect-transmission point $\vec{Q}=\vec{0}$ has a nonlocal effect on the system. When we adiabatically change the parameters $\vec{Q}$ along a cycle around $\vec{Q}=\vec{0}$, where the transmittance T vanishes, one unit of charge e can be pumped and leads to the polarization change by $\pm 2ea$ according to Brouwer's formula (a is the lattice constant and $2a$ is the size of the unit cell) [Eq. (16)]. In this unit, the total vorticity N_v corresponding to the polarization is defined to be 1. The vortex is almost isotropic, at least in the vicinity of its core. Then, a pumped charge due to a small change $\vec{\Delta}$ of $\vec{Q}$ is expressed as $q \sim (\phi/2\pi)e \sim (|\vec{\Delta}|/E_G)e$, where ϕ is the change in the polar angle of the vector $\vec{Q}$. This quantized charge pumping[8] through the adiabatic cyclic change of $\vec{Q}$ is consistent with the results previously found in the periodic system[6] by using the Berry-curvature formulation of the electric polarization.[1]

Now, we introduce the disorder. In the $\vec{Q}$ plane, the region of $|\vec{Q}| \lesssim v$ becomes gapless, while the Anderson localization dominates the transport properties.[15,29] Especially in one dimension, the effect is pronounced and all the states are localized.[30–32] On the other hand, the total vorticity N_v is an integer topological number, which is robust under a continuous change of parameters including the disorder strength when the gap does not collapse. Therefore, even with disorder, N_v remains unity. Namely, there exists at least one vortex ($r=0$) in the $\vec{Q}$ plane. The perfect transmittance $|t|=1$ occurs even when all the states are strongly localized. This is a remarkable consequence from the quantum and topological property, which is in sharp contrast to the usual classical tunneling through disordered insulators.

In Figs. 3(a2) and 3(b2), we show our numerical results of R and φ for $L=101$, with the uniform random distribution $v_i \in [-v, v]$ for the disorder strength $v=0.25t_{nn}$. We observe that the vortex center of the perfect transmittance $T=1$ and $R=0$ shifts in the $\vec{Q}$ space. In addition, an anisotropy develops in the shape of the region of relatively high transmittance T. We further calculate R and φ for larger systems, which are shown in Figs. 3(a3) and 3(b3) for $L=201$ and in Figs. 3(a4) and 3(b4) for $L=401$. It is clear that the vortex core, which is almost isotropic without the disorder, rapidly evolves into the highly anisotropic one. This is associated with an increase of the ratio L/ξ by increasing the system size. Figure 4 shows the local density of states D_i of site $i(=1, \ldots, L)$, which has been calculated when $\vec{Q}$ is located at the vortex center $\vec{Q}_c$ corresponding to each case of $L=101$, 201, and 401 for $v/t=0.25$. When L is equal to 101 or smaller, the state at this energy is extended over the sample. However, with increasing L, the state is almost localized in the middle of the sample. The spatial extension of the wave function, i.e., the localization length ξ, can be explicitly evaluated from the second moment of D_i as the inverse participation ratio,

$$\xi_{IPR} = \left(\sum_i D_i \right)^2 \Big/ \sum_i D_i^2. \qquad (19)$$

We obtain $\xi_{IPR}=51.4$, 80.8, 76.4, and 84.7 for $L=101$, 201, 401, and 501, respectively, around the vortex center, indicat-
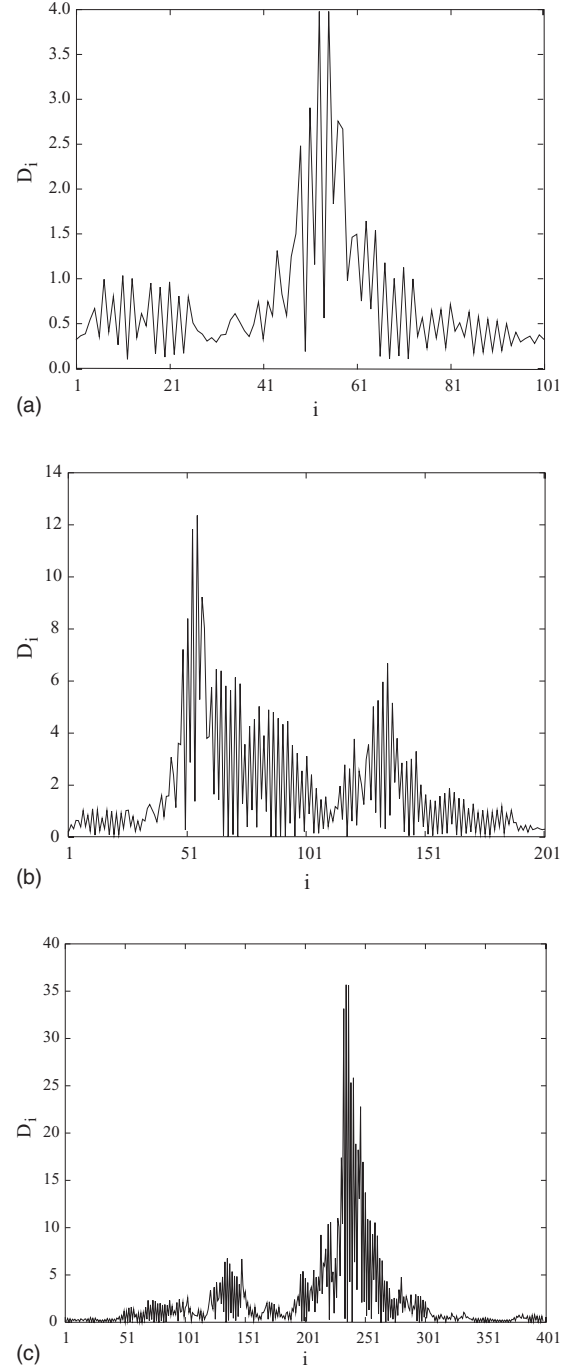

(a)

(b)

(c)

FIG. 4. Local probability D_i of the state at the vortex for (a) $L=101$, (b) $L=201$, and (c) $L=401$ in the presence of uniformly distributed random potential $v_i \in [-v, v]$, with $v=0.25t_{nn}$.

ing that ξ_{IPR} almost saturates about 80 sites for $v/t=0.25$. Furthermore, in this anisotropic "wing," φ changes rapidly. The width Q_W of the anisotropic wing decays exponentially as $\exp(-L/\xi)$ with increasing L, as shown in Fig. 5.

Let us briefly comment on the relation of the charge displacement discussed above to the charge pumping through the quantum dot[20] connected by two leads. When the system has a finite conductance, the main source of the pumping is contributed both from the transmission and from the reflection coefficients. Therefore, it is not topologically quantized.
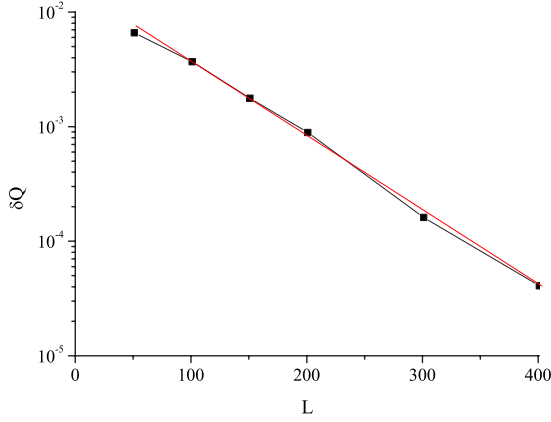
FIG. 5. (Color online) The minimum width δQ for R determined at $R=0.3$ as a function of L.

However, by increasing the system size, it may cross over to the insulating regime, especially in the presence of the disorder. We will show that in this case the charge pumping topologically comes from the vortex of the reflection coefficient. Namely, the vortex is topologically protected against the disorder. The topological constraint guarantees the charge pumping, which can be understood by the resonance tunneling[33] near the vortex.

B. Resonance tunneling

In order to understand transport properties of such one-dimensional disordered systems, it is sometimes useful to consider an effective model, with the potential having high double peaks. In this model, well-defined localized eigenstates exist between the two potential peaks, and any transport between two ends of the system occurs via the localized states through tunneling. While such tunneling has an exponentially small probability, it occurs when the Fermi energy of the leads is equal to one of the eigenenergies of the localized states, namely, when the resonance takes place. This picture of transport in disordered systems is called "resonance tunneling.[33]"

Following Ref. 33, we develop the resonance-tunneling theory for our case. We define an effective model of resonance tunneling, as described by the Schrödinger equation $\Psi''(x)+[k^2-V(x)]\Psi(x)=0$, where $\hbar^2 k^2/2m$ is the kinetic energy, and the effective potential $V(x)$ has two peaks, as shown in Fig. 6. Although it is not trivial to derive the effective potential from the on-site randomness, our numerical results can be fitted well using the effective potential when the localization length ξ is much shorter than the system size. The tunneling is guaranteed by the perfect-transmittance point protected by the topology; i.e., the resonant tunneling in the two-dimensional parameter space (Q_1, Q_2) takes place in spite of the complexity of the potential shape in the model.

First, let us consider an open system attached to two ideal leads, which are connected to reservoirs. The Fermi energy E_F is tuned at one's disposal, and we assume that the potential peaks are much higher than E_F. An effective wave number $k(x) \equiv \sqrt{k^2 - V(x)}$ becomes imaginary inside the potential peaks, and the particle tunnels through the peaks. One of the
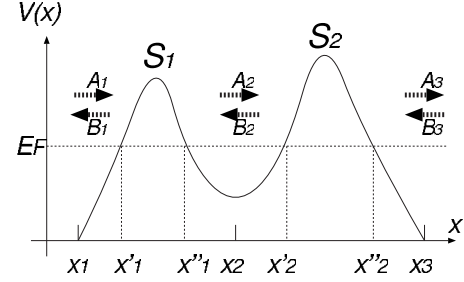

FIG. 6. Potential profile for the effective model of resonance tunneling. Heights of the two potential peaks are characterized by S_1 and S_2.

eigenstates in the left lead $(x<x_1)$ is given by $\Psi_1(x) \sim \exp[ik_1(x-x_1)]$, where $k_1=k(x_1)$. The time-reversal symmetry of the system requires that the complex conjugate $\Psi_1^*(x)$ is also an eigenstate. At the potential valley around $x=x_2$, we can also consider eigenstates with $\Psi_2(x) \sim \exp[ik_2(x-x_2)]$ and $\Psi_2^*(x)$, where $k_2=k(x_2)$. Thus, general eigenstates around $x=x_1$ and around $x=x_2$ are given as $\Psi(x)=A_1\Psi_1(x)+B_1\Psi_1^*(x)$ and $\Psi(x)=A_2\Psi_2(x)+B_2\Psi_2^*(x)$, respectively. Next, we introduce the transfer matrix Θ_1 from x_2 to x_1,

$$\begin{pmatrix} A_1 \\ B_1 \end{pmatrix} = \Theta_1 \begin{pmatrix} A_2 \\ B_2 \end{pmatrix}, \quad (20)$$

where Θ_1 is a 2×2 matrix. The time-reversal symmetry requires the transfer matrix Θ to be of the form

$$\Theta_1 = \left(\frac{k_2}{k_1}\right)^{1/2} \begin{pmatrix} \cosh(S_1)e^{i\alpha_1} & \sinh(S_1)e^{i\beta_1} \\ \sinh(S_1)e^{-i\beta_1} & \cosh(S_1)e^{-i\alpha_1} \end{pmatrix}. \quad (21)$$

In a semiclassical theory, we have

$$\alpha_1 = -\int_{x_1}^{x_1'} k(x)dx - \int_{x_1''}^{x_2} k(x)dx, \quad (22)$$

$$\beta_1 = \frac{\pi}{2} - \int_{x_1}^{x_1'} k(x)dx + \int_{x_1''}^{x_2} k(x)dx. \quad (23)$$

S_1 characterizes the height of the potential, as the transmission coefficient t_1 is given by $t_1=e^{i\alpha}\operatorname{sech} S_1$. Since we have assumed that the peak is high, which means $S_1 \gg 1$, the transmission probability $|t_1|^2$ is then approximated as $|t_1|^2 \sim 4e^{-2S_1} \ll 1$.

Similarly, we introduce the transfer matrix for the second peak as

$$\begin{pmatrix} A_2 \\ B_2 \end{pmatrix} = \Theta_2 \begin{pmatrix} A_3 \\ B_3 \end{pmatrix}, \quad (24)$$

and we have

$$\Theta_2 = \left(\frac{k_3}{k_2}\right)^{1/2} \begin{pmatrix} \cosh(S_2)e^{i\alpha_2} & \sinh(S_2)e^{i\beta_2} \\ \sinh(S_2)e^{-i\beta_2} & \cosh(S_2)e^{-i\alpha_2} \end{pmatrix}. \quad (25)$$

The phases α_2 and β_2 can be written similarly to α_1 and β_1, where $S_2 \gg 1$. We assume that S_i, α_i, and β_i $(i=1,2)$ are smooth functions of the parameters Q_1, Q_2, and E_F. A trans-

(a1) phase of r (small S₁,S₂)   (a2) phase of r ' (small S₁,S₂)

(a3) charge motion

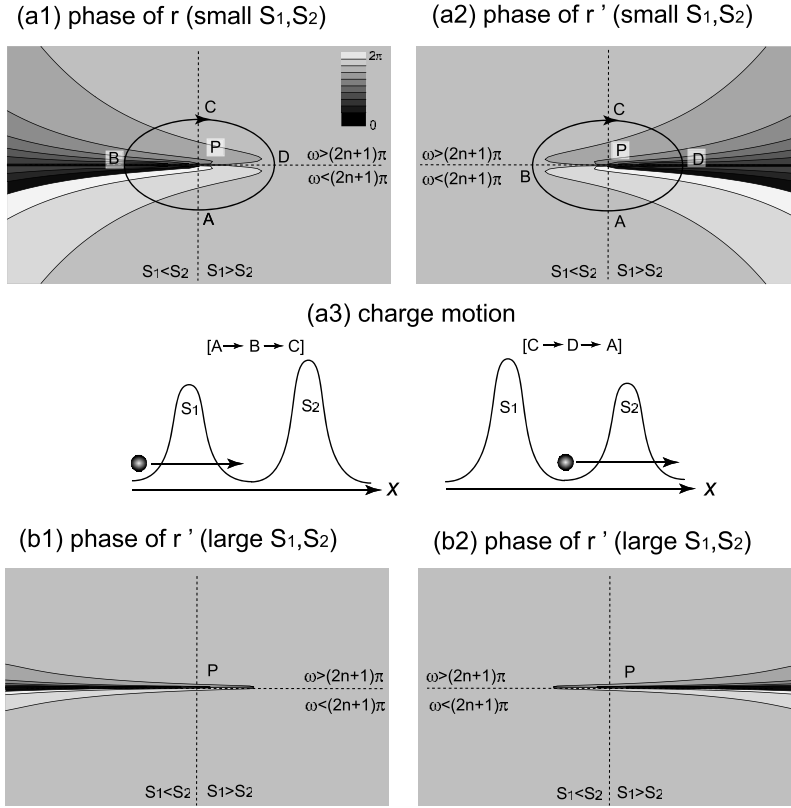(b1) phase of r ' (large S₁,S₂)   (b2) phase of r ' (large S₁,S₂)

FIG. 7. Schematic contour mapping of the phases of the reflection coefficients r and r' in the Q_1-Q_2 plane. (a1) and (a2) correspond to small S_1 and S_2, and (b1) and (b2) to large S_1 and S_2. The phases of r and r' wind by 2π during the cycle around the "vortex" P. When we go along the arrows indicated in (a1) and (a2), the phase of r (r') increase by 2π (-2π). (a3) illustrates the motion of the charge in the cycle. Note that the 2π phase change of r (r') is associated with pumping one unit charge into the system through the left (right) end of the system.

fer matrix Θ for the entire system is given by

$$\Theta = \Theta_1 \Theta_2 = \left(\frac{k_3}{k_1}\right)^{1/2}\begin{pmatrix} \theta_{11} & \theta_{21}^* \\ \theta_{21} & \theta_{11}^* \end{pmatrix}, \tag{26}$$

$$\theta_{11} = e^{i(\alpha_1+\alpha_2)}(\cosh S_1 \cosh S_2 + \sinh S_1 \sinh S_2 e^{i\omega}), \tag{27}$$

$$\theta_{21} = e^{i(\alpha_2-\beta_1)}(\sinh S_1 \cosh S_2 + \cosh S_1 \sinh S_2 e^{i\omega}), \tag{28}$$

$$\omega = \beta_1 - \beta_2 - \alpha_1 - \alpha_2 \cong 2\int_{x_1''}^{x_2'} k(x)dx. \tag{29}$$

From the unitarity, it follows that $|\theta_{11}|^2 - |\theta_{21}|^2 = 1$. We also assume that the Fermi energies of the two leads are identical, which means $k_3 = k_1$. For a plane wave incident from the left lead, we denote r and t as the reflection and transmission coefficients, respectively. Similarly, for a plane wave from the right lead, we define r' and t' as well. We then obtain

$$r = \theta_{21}/\theta_{11}, \quad t = t' = 1/\theta_{11}, \quad r' = -\theta_{21}^*/\theta_{11}. \tag{30}$$

It implies the unitarity $|r|^2 = |r'|^2 = 1 - |t|^2$. It also satisfies $t = t'$ and $rt^* + r'^*t = 0$, as required by the time-reversal symmetry.

We now apply this framework to fit our numerical results. Because r is written as

$$r = e^{i\theta}\frac{\tanh S_1 + \tanh S_2 e^{i\omega}}{1 + \tanh S_1 \tanh S_2 e^{i\omega}}, \tag{31}$$

a condition for a total transmission, $r=0$, is given by

$$S_1 = S_2, \tag{32}$$

$$\omega = 2\int_{x_1''}^{x_2'} k(x)dx = (2n+1)\pi, \tag{33}$$

where n is an integer. The latter condition is equivalent to the Bohr quantization condition that the state localized around x_2 be an eigenstate with its eigenenergy equal to E_F. In other words, the total transmission occurs at resonance. For the fixed E_F, the two conditions (32) and (33) define the isolated points in the Q_1-Q_2 plane. Let P denote one of such points of total transmission: $r=0$. One can easily see that around point P, the phase of r and that of r' wind by $\pm 2\pi$, as schematically shown in Figs. 7(a1) and 7(a2). From the Brouwer formula (16), the phase windings of r and r' correspond to (2π times) the amount of charge pumped into the system through the left and right ends, respectively. Thus, by going around point P, one unit charge is pumped from the left lead to the right. For illustration, let us consider a clockwise cycle around point P in Figs. 7(a1) and 7(a2). This pumping from left to right is analogous to the "bicycle pump."[28] The two potential peaks correspond to two gates to control the pumping. If the system crosses the line $\omega=(2n+1)\pi$ at the $S_1 < S_2$ side, r undergoes 2π phase changes. It means that tunneling occurs through the left potential peak due to the resonance, corresponding to the opening of a "left gate," and a
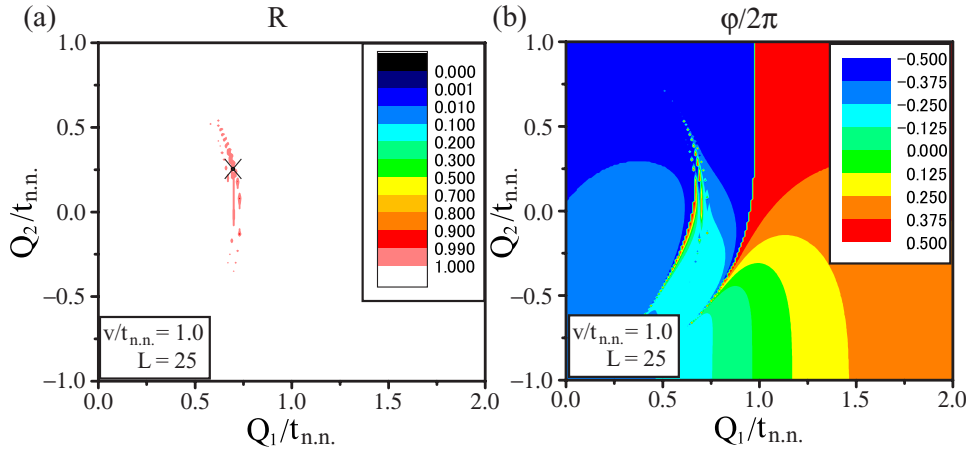
FIG. 8. (Color online) (a) Reflectance and (b) the phase φ of r in a disordered system with $L = 25$ and $v/t_{nn} = 1.0$ for the alloy model with the on-site random potential given in Fig. 2.

unit charge flows in. After that, the left gate closes, and the right gate opens in turn, when the system crosses the line $\omega = (2n+1)\pi$ at the $S_1 < S_2$ side, and r' undergoes a -2π phase change. The charge is pumped to the right lead after one cycle. Thus, the overall motion of the charge is as shown in Fig. 7(a3). For the pumped charge to be quantized, the cyclic process should be sufficiently slow to be regarded as "adiabatic." Otherwise, the particle cannot tunnel through the potential barriers. Below, let us make this physical picture more explicit in relation to our numerical results.

In our numerical results in Figs. 3(b2)–(b4), the phase-winding point P corresponds to the perfect transmission. When we go from Fig. 3(b2) to Fig. 3(b4), L/ξ increases. In the resonance-tunneling picture, it means that S_i increases and that the "resonance-tunneling wing" narrows, as seen by comparing Figs. 7(a1) and 7(b1). It is exactly observed in our numerical results.

For large L/ξ, the transmission probability $|t|^2$ is typically $\sim e^{-2(S_1+S_2)} \sim e^{-2L/\xi}$. Because we have $S_1 \sim S_2$ near the resonance, we estimate $S_1 \sim S_2 \sim (L/2\xi)$. In that case, the change of the phases of r and r' occurs abruptly at around $|\omega - (2n+1)\pi| \sim e^{-L/\xi}$. Along the line $\omega = (2n+1)\pi$, $|r|$ is given by $|r| = \tanh(S_1 - S_2)$, which becomes appreciable only when $|S_1 - S_2| \sim 1$. This is found only in a small region $\Delta/t_{nn} \sim \xi/L$. When $L/\xi \gg 1$, because the tunneling rate Q_W is exponentially small ($Q_W \sim t_{nn} e^{-L/\xi}$), charge pumping requires an exponentially long time $\tau \sim (\hbar/t_{nn})e^{L/\xi}$. This is the time scale which gives a criterion for adiabatic charge pumping in this system. If one changes the parameters faster than this time scale, the pumped charge is reduced by an exponential factor $e^{-\omega/E_G}$ as a nonadiabatic correction, where ω is a frequency of the change of the external parameters.[34]

Generally, there occurs no perfect-transmittance point by tuning only two parameters since the effective two-barrier model for the resonant tunneling applies only to a limited region of the random system and not through a whole sample. In the present case, it is guaranteed by the topological constraint that the phase of $r(r')$ should wind by $(-)2\pi$ for a large cycle far from $\vec{Q} = 0$, well within the gapped region.[9] When $|\vec{Q}|$ is larger than the energy scale of the disorder, a finite gap $(\sim |\vec{Q}|)$ opens. The wing will then become as wide as $Q_W \sim |\vec{Q}|$. Correspondingly, the typical time scale

$\tau \sim \hbar/Q_W \sim \hbar/|\vec{Q}|$ becomes smaller, and the adiabaticity condition is easily satisfied. In such case, however, the dielectric response is not enhanced. The localization length becomes as long as the system size, and the pumping is accomplished through extended states, not by resonance tunneling. Remarkably, this charge pumping in the gapped region is governed by the vortex which is located deep in the disordered regime ($\xi \ll L$). In other words, the charge pumping in the gapped regime ($\xi \sim L$) is smoothly connected to that via resonance tunneling in the disordered regime ($\xi \ll L$). We note that S_1 and S_2 are regarded as effective parameters, although the real potential is much more complicated than the two-barrier structure.

C. Multichannel problem in an alloy model for an on-site random potential

In the rest of this section, we consider a stronger randomness by employing the alloy model [Fig. 2(b)] with $v_i = s_i(v + \delta v_i)$, with $s_i = \pm 1$ being a random sign and $\delta v_i/v \in [-0.025, 0.025]$ a uniform random distribution, instead of the uniformly distributed random potential [Fig. 2(a)].

Let us start with the single-channel case. Then, for a fixed disorder strength v, the shape of the vortex core of the reflection coefficient rapidly evolves from isotropic to anisotropic with the increasing system size L, as in the case of the uniformly distributed random potential discussed in Sec. III A. This tendency is generic and also realized for a fixed system size L with the increasing disorder strength v. In Figs. 8(a) and 8(b), we show the reflectance R and the phase φ in the $\vec{Q}$ space for $v/t_{nn} = 1.0$ and a small sample size $L = 25$. Here, the region in the $\vec{Q}$ plane where the gap collapses and vortices distribute expands because of the stronger disorder and thus the much shorter localization length $\xi \sim 3$ or 4. The transmittance T is typically obtained as $\sim 10^{-9}$, which is practically negligible except at the vortex core.

Now, we consider a system that consists of many channels, each of which is described by the present disordered alloy model, but with a different profile of random potentials. Such configuration can be realized in thin films of ferroelectrics. Then, we can design the pattern of the phase φ in the $\vec{Q}$ plane by tuning the disorder. For the alloy model with the
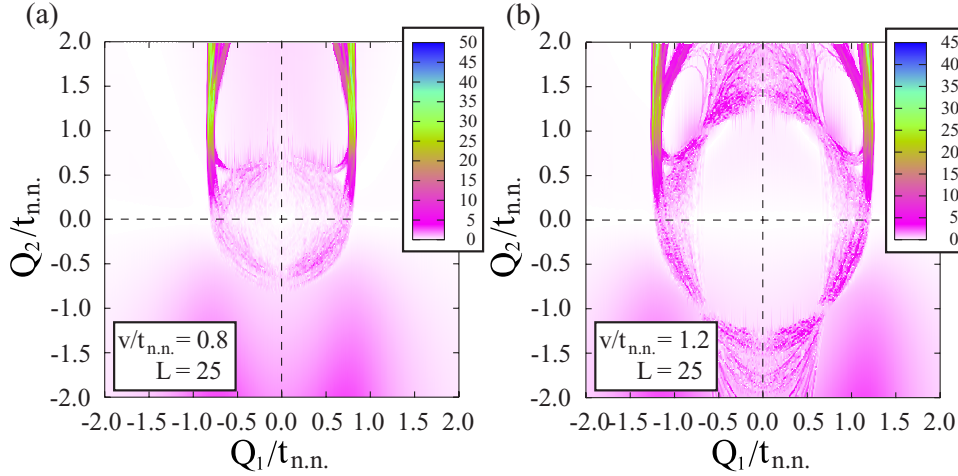
FIG. 9. (Color online) Relative dielectric response in the presence of the disorder compared with the pure case. The disorder strength is $v/t_{nn}=0.8$ for (a) and 1.2 for (b). Averages are taken over 10^2 random disorder configurations. Inside white bands, there occurs a gradual sign change in the dielectric response.

random on-site potentials, vortices are mostly located around $Q_1=\pm v/2$, with the wing almost along the Q_2 axis. Therefore, we can enhance the dielectric response if we can tune the disorder strength and choose a sample where the $\vec{Q}$ point of the system is located inside the wing. In particular, when the transmittance T is negligibly small, the enhancement factor of the dielectric response is given by $(\partial\varphi/\partial\theta)_{\text{disorder}}/(\partial\varphi/\partial\theta)_{\text{pure}}$ from Eq. (16) since the electric field is proportional to $\theta=\arctan(Q_1/Q_2)$. We calculate this enhancement factor for this multichannel system, increasing the number N of channels. Figures 9(a) and 9(b) represent the $\vec{Q}$ dependence of the enhancement factor in the case of $v/t_{nn}=1.6$ and 2.4, respectively, for $L=25$ with $N=102$. The main structure in this map is almost saturated up to $N=10^2$. These results reveal that around $Q_1\sim\pm v/2$, the dielectric response is significantly enhanced by a factor of 30–40 compared with the pure case. Even for the thin film with a square shape of a linear dimension larger than 50 Å, which corresponds to $N=10^2$, the disorder-induced enhancement of the charge transfer rate should be robust. Then, the applied electric field necessary for switching the polarization is reduced by this enhancement factor. If we require the response time $\tau\sim e^{L/\xi}/t_{nn}$ of the order of 10^{-9} s, we obtain $e^{L/\xi}<10^6$ with the assumption of $t_{nn}\sim10^{15}$ s^{-1}. This also assures a negligibly small transmittance $T\sim e^{-L/\xi}\sim10^{-6}$ and, thus a small leak current and low dissipation.

Possible experimental realization of this quantum-mechanical disorder-induced enhancement of the dielectric response, namely, the quantum relaxor, has also been proposed[10] for thin films of solid solution systems such as Pb(Fe$_{0.5}$Nb$_{0.5}$)O$_3$ and Pb(Sc$_{0.5}$Nb$_{0.5}$)O$_3$ prepared with an adequate slow-annealing process.[35,36]

IV. PERIODIC/TWISTED BOUNDARY CONDITION

The adiabatic charge pumping in the presence of the substrate disorder was considered by Niu and Thouless.[9] They showed that the adiabatic charge transport is still quantized as long as the excitation gap between the highest occupied molecular orbital (HOMO) and the lowest unoccupied molecular orbital (LUMO) does not vanish with respect to the substrate disorder and the many-body interaction in the thermodynamic limit. In the case of an open boundary condition, it is easy to imagine the meaning of charge pumping: the charge transport from one end to the other. In the case of the periodic boundary condition, the charge pumping after one cycle refers to the electronic wave function to shift by one unit cell. A cartoon picture of this process is given in Fig. 10. We note that in the absence of the disorder, the adiabatic charge transport has been related to the field-theoretical model of the one-dimensional chiral anomaly.[37]

A. Formalism

In contrast to the open system with two leads, we solve the closed system in a ring geometry. Moreover, we introduce a twisted boundary condition by applying a magnetic flux through the one-dimensional ring. In the pure case, the lattice momentum k is a good quantum number, and the parameter space is three-dimensionally spanned by (Q_1,Q_2,k). However, in the disordered case, k is no longer a good quantum number. The parameter space becomes (Q_1,Q_2,α), with $\alpha\in[0,2\pi]$. The Hamiltonian is given by

$$H(\alpha)=-\frac{t_{nn}}{2}\sum_{j=1}^{N}(e^{i\alpha/N}c_j^\dagger c_{j+1}+\text{H.c.})+Q_1\sum_{j=1}^{N}(-1)^j c_j^\dagger c_j$$

$$+\frac{Q_2}{2}\sum_{j=1}^{N}(-1)^j(e^{i\alpha/N}c_j^\dagger c_{j+1}+\text{H.c.})+V, \qquad (34)$$

where $c_{N+1}\equiv c_1$ and $V=\Sigma_j v_j c_j^\dagger c_j$ is the uniformly distributed disorder potential.
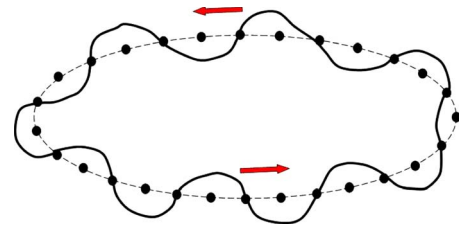

FIG. 10. (Color online) A cartoon picture of the charge transport on the one-dimensional ring.

In the tight binding model, the polarization operator $\vec{P}$ has the following form:

$$\vec{P} = \sum_j \vec{R}_j c_j^\dagger c_j, \tag{35}$$

where $\vec{R}_j$ is the position vector at site j and $c_j^\dagger c_j$ is the electron density operator. The current is defined by the time derivative of the polarization operator given by

$$\vec{J} = \frac{\partial \vec{P}}{\partial t} = \frac{1}{i}[\vec{P}, H]. \tag{36}$$

In the pure case, the current is given by $\frac{\partial H}{\partial k}$, whereas in the present case with disorder, the current operator given by $\frac{\partial H}{\partial \alpha}$ has the following form:

$$J = ie^{-i\alpha/N} \sum_j [t + Q_2(-1)^j] c_{j+1}^\dagger c_j + \text{H.c.} \tag{37}$$

When the flux α is equal to 0 or π, the system is time-reversal symmetric, and there is no persistent current. In such cases, we can consider a change of the electric polarization by an adiabatic change of parameters Q_1 and Q_2. In the linear response theory, the change of the electric polarization is given by

$$\delta P = F_1 \Delta Q_2 - F_2 \Delta Q_1, \tag{38}$$

with

$$F_1 = -\frac{i}{L} \sum_{m \neq 0} \left(\frac{\langle \Psi_0 | J | \Psi_m \rangle \langle \Psi_m | \frac{\partial H}{\partial Q_2} | \Psi_0 \rangle}{(E_m - E_0)^2} - \text{c.c.} \right), \tag{39}$$

$$F_2 = \frac{i}{L} \sum_{m \neq 0} \left(\frac{\langle \Psi_0 | J | \Psi_m \rangle \langle \Psi_m | \frac{\partial H}{\partial Q_1} | \Psi_0 \rangle}{(E_m - E_0)^2} - \text{c.c.} \right), \tag{40}$$

where $L = Na$ is the circumference of the ring (where a is the lattice spacing) and

$$\frac{\partial H}{\partial Q_1} = \sum_j (-1)^j c_j^\dagger c_j, \tag{41}$$

$$\frac{\partial H}{\partial Q_2} = \frac{1}{2} \sum_j (-1)^j (e^{i\alpha/N} c_j^\dagger c_{j+1} + e^{-i\alpha/N} c_{j+1}^\dagger c_j). \tag{42}$$

We note that the change of the polarization δP is generally dependent on the path in the parameter ($\vec{Q}$) space. The $|\Psi_0\rangle$ in Eqs. (39) and (40) is the many-body ground state, and $|\Psi_m\rangle$ denote the excited states. E_0 and E_m are the energy for the ground and excited states, respectively. In the pure case, when the chemical potential lies in the gap, the system is a band insulator. The magnitude of the energy gap is given by the magnitude of the charge-density-wave order parameter (Q_1, Q_2). In the presence of the disorder, the gap closes when the magnitude of the disorder potential becomes the order of

$\mathcal{O}(\sqrt{Q_1^2 + Q_2^2})$. The system remains insulating because each state is localized, i.e., Anderson localization.

Although we defined Eqs. (38)–(40) only for $\alpha = 0$ and $\alpha = \pi$, it can be generalized to any α easily. We should note that except for $\alpha = 0$ and π, $\delta P(\alpha)$ does not mean a change of polarization. With the extension to arbitrary α, let us succinctly abbreviate (Q_1, Q_2, α) as $\vec{Q} = (Q_1, Q_2, Q_3)$ and define the gauge potential as

$$\vec{A} = i \left\langle \Psi_0 \left| \frac{\partial}{\partial \vec{Q}} \right| \Psi_0 \right\rangle. \tag{43}$$

This gauge field is defined so that the corresponding field strength $\vec{F} = \nabla \times \vec{A}$ has the components given in Eqs. (40) and (39). Furthermore, when the parameters (Q_1, Q_2) are changed along a cycle, the pumped charge can be written as

$$\delta P(\alpha) = \oint_S d\vec{Q} \times \hat{\alpha} \cdot \vec{F}(\vec{Q}), \tag{44}$$

where S is a loop on the $Q_1 - Q_2$ plane. Using the Stoke's theorem, Eq. (44) becomes

$$\delta P(\alpha) = \int d^2 Q D(\vec{Q}), \tag{45}$$

where $D(\vec{Q}) = \partial_1 F_1 + \partial_2 F_2$ is defined as the distribution function of the polarization. This pumped charge is not necessarily an integer. However, in a strongly disordered system it becomes an integer, with an exponentially small correction of the order of $e^{-L/\xi}$. To see this, we note that the wave functions in a strongly localized case are almost insensible to the twisted boundary condition α within an accuracy of $e^{-L/\xi}$. Hence, $\Delta P(\alpha)$ is equal to an average $\Delta P(\alpha)$ over α, namely,

$$\Delta P = \int_0^{2\pi} \frac{d\alpha}{2\pi} \Delta P(\alpha) = \int_{\partial T} d\vec{\sigma} \cdot \vec{F}, \tag{46}$$

where ∂T is the torus surface and $d\vec{\sigma}$ is the surface element. This average ΔP represents the total flux over a torus surface, and it is an integer, which follows from topological properties of the gauge field $\vec{A}$. As the field strength is defined as $\vec{F} = \nabla \times \vec{A}$, it satisfies $\nabla \cdot \vec{F} = 0$ *if there is no singularity, i.e., there is no energy crossing*. Thus, when there are no energy degeneracies inside the torus $V \times [0, 2\pi]$, the averaged pumped charge ΔP becomes zero due to the Gauss theorem. If there is an energy crossing, the gauge field $\vec{A}$ has a U(1) monopole there, and the averaged charge ΔP becomes a total strength of the monopoles inside the torus, again by using the Gauss theorem. As the monopole strength is quantized to be an integer, ΔP is always an integer. This discussion for Eq. (46) corresponds to that for Eq. (2.23) in Ref. 9, in which they claimed that the charge transport is quantized in the presence of a gap which does not vanish in the thermodynamic limit. On the other hand, the aim of this paper has another target: we are interested in the strong disorder case, in which the energy gap closes in the thermodynamic limit and all wave functions are localized and characterized by the localization length ξ defined by $\xi^{-1} = \int dx |\psi(x)|^4$,

where ψ is the single particle wave function. Nevertheless, for the finite-size system, a gap always exists, which is the order of the band width divided by the size of the system. Therefore, it validates the above topological argument even in the strongly disordered cases. In such disordered systems, the field strength $\vec{F}$ is highly anisotropic around the monopoles, which is closely related to a resonance tunneling picture in Sec. III B.

The adiabatic charge transfer is based on the occurrence of the singularity in the parameter space,[6] which happens when LUMO and HOMO are degenerate. By making a close contour enclosing the singularity, the wave function shifts, as shown in Fig. 10. Since the disorder potential is random, we expect that the proliferation of the singularities may occur. Furthermore, there could be a *singularity string* rather than a *point* in the strong disorder limit. The reason is given as follows. In the strong disorder limit, all wave functions are localized. There could be a situation that the wave functions of the LUMO and the HOMO are well separated so that the overlap integral of the two wave functions are exponentially small as the parameters change. Thus, even when the change of parameters in numerics or in experiments is very slow, its time scale might still be shorter than the inverse of the (exponentially small) overlap integral of the LUMO and HOMO. Therefore, within this variation of parameters, the LUMO and HOMO can be regarded as a degenerate. Once they are degenerate at a certain point in the parameter space, they will keep the near degeneracy as the parameters change until their wave functions have an appreciable overlap and open a gap. As long as they remain nearly degenerate as the parameters change, the singularity string is created in the parameter space. Moreover, because the wave functions are highly localized on the singularity string, they are *insensitive to the boundary condition*, in other words, α independent. Therefore, they have a sheetlike structure extending along the α direction in the parameter space. Even though it is sheetlike, we call it a string, referring to its projection on the (Q_1, Q_2) plane. From this observation, we conclude that the singularity in the parameter space projected on Q_1 and Q_2 subspaces has two kinds, points and strings, in the strong disorder limit. The former contribute to the charge transfer, while the latter do not. The charge transfer for the former is explained within the resonance tunneling (Sec. IV C).

B. Numerical results

In this section, we solve numerically the eigenvalue problem for slowly varying parameters (Q_1, Q_2) and calculate the contour integral in Eq. (44). We introduce the small segment $\Delta\vec{Q}$ for the contour integral and demand that F_1, F_2 are continuous. Therefore, the size $|\Delta\vec{Q}|$ determines the energy scale and time scale of our simulation. In an actual calculation, we take $|\Delta\vec{Q}| = 10^{-6} t_{nn}$ as the finest one. Then, the discussion below applies when we observe the system within the time scale $T \sim \hbar/|\Delta\vec{Q}| \sim 10^6 \hbar/t_{nn}$. Also, we average over α to see the quantization of the charge transfer in Eq. (46).

We solve Eq. (34) by a direct numerical calculation. Our goal is to compute the distribution function from Eq. (45),
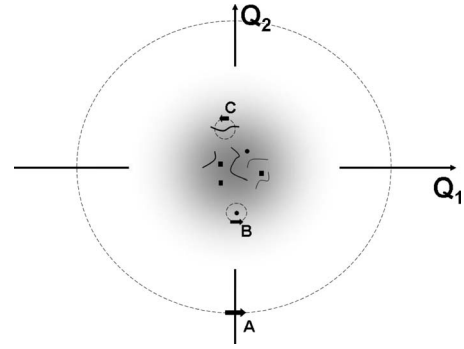

FIG. 11. A cartoon picture of the distribution of singularities at $\alpha=0$. The singularity has two kinds: strings and points. Calculating Eq. (44) from the outer big dash loop gives the polarization +1.0 and −1.0 from the loop B. If we stay far away from the origin, one would think that there is only one monopole with $\Delta P = 1.0$ at the center, like in the pure case. However, when the disorder strength is strong enough, there are some subtle structures inside the big monopole. There are the monopole-antimonopole pairs and the singularity strings.

which is α dependent. We will also demonstrate the quantization of the charge transfer by averaging over α by Eq. (46).

We consider a ring with $N=50$ and take v_i/t_{nn} to distribute uniformly in $[-7.0, 7.0]$. To obtain the distribution function, we divide the (Q_1, Q_2) plane into small pieces of grids and calculate Eq. (45) for each grid. Let us remind the readers that the distribution function for the pure case is the δ-function at the origin.[6] In that case, we do not need to integrate over α to obtain the quantization of the charge transfer because the singularity lives in the (Q_1, Q_2, k) space, and the integration over k is already included implicitly in Eq. (45).

Our result can be summarized by the cartoon in Fig. 11. First, we found that $\Delta P = 1.0$ if we take loop A, which is the outer dash one $(|\vec{Q}| \sim 10)$, and average over α. It corresponds to the weak disorder case where the strength of the disorder is much smaller than $|\vec{Q}|$, so the potential strength is not large enough to close the gap. According to Niu and Thouless,[9] the polarization is quantized, and we reproduce their result here. Secondly, the singularity strings appear in the region $|\vec{Q}| \leq 4.5$. In this region, the disorder potential is strong enough to close the gap. As we pointed out in Sec. IV A, there are two kinds of singularities, points, and strings. In the "stringful" region, it is rather difficult to locate the singularity point. It is because the operation of the adiabatic process changes when making the contour across a string. In Fig. 12, we illustrate two different adiabatic processes regarding making contours enclosing the singularity points and across the singularity string. Figure 12(a) shows the usual definition of the adiabatic process. In the presence of the gap, the adiabatic process has to follow the lower energy state, which is indicated by the square dots in Fig. 12(a). Figure 12(b) shows the adiabatic process of the contour across the string. In this case, because the wave functions of the HOMO and the LUMO do not overlap, the adiabatic process needs to keep ramping up to the higher energy state at the first degenerate point and to keep ramping down to the lower energy
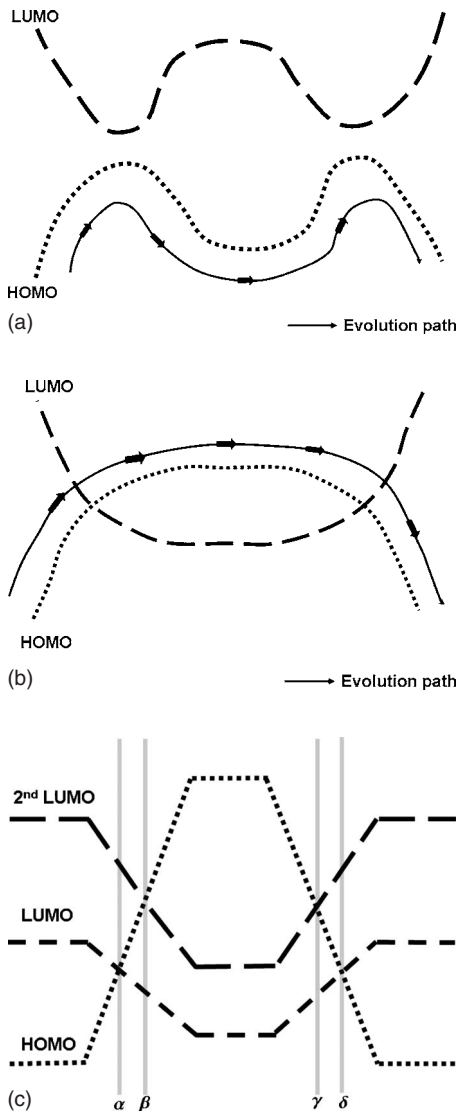
FIG. 12. The adiabatic process in the gapless case is different from the gap case. (a) shows the process with a gap. (b) shows the process without a gap. (c) shows a real process from loop C in Fig. 11.

state at the second degenerate point, which completes a close loop. Note that the energy of the HOMO is larger than that of the LUMO after the first degenerate point and becomes smaller again after the second degenerate point. In other words, the system stays in the same state, and thus the charge does not transfer at all after a close contour. Therefore, even if we make a close loop which encloses a whole singularity string, the charge does not transfer. It should be noted that even though the system is at a higher energy state, it takes $\sim e^{L/\xi}$ to relax, where L is the size of the system and ξ is the typical localization length which is around three sites in our case.

In Fig. 12(c), we demonstrate a real process across a singularity string indicated by loop C in Fig. 11. Usually, we refer the singularity string to the degenerate manifold between the HOMO and LUMO. In a real process, we may have to consider the degeneracy between the HOMO and the second LUMO. For example, after the degenerate point be-

tween the LUMO and HOMO, the descending order in energy is the second LUMO, the HOMO, and the LUMO. There is the possibility, for example, the boundary β in Fig. 12(c), that the energy of the second LUMO and that of HOMO can be the same along the contour before meeting the next degenerate point between the HOMO and LUMO. If it happens, the system still stays in the original HOMO state by ramping further up to the higher energy state. After that, the descending order in energy becomes the HOMO, the second LUMO, and the LUMO. Figure 12(c) shows the complete process, and the system has to go back to its original state after completing a close loop. As a result, HOMO, LUMO, and other states can be viewed as the Riemann sheets. Singularity strings are like the branch cuts which connect different Riemann sheets. Contours on the (Q_1, Q_2) plane are very similar to the one in the complex plane.

As the string just corresponds to the degenerate states, which does not penetrate through the whole sample, the only topological object which contributes to the polarization is the isolated singularity point. We found one at $(Q_1, Q_2, \alpha) = ($−0.3885, −4.804 15, 0). If we calculate Eq. (46) around that point, for example, loop B in Fig. 11, we obtain $\Delta P = -1.0$. We identify the singularity point which carries $\Delta P = -1.0$ with the antimonopole in contrast to the monopole which carries $\Delta P = 1.0$. Considering the total flux calculated from loop A in Fig. 11 to be 1.0, there must be at least two monopoles and one antimonopole in our system, which demonstrates the proliferation of the monopole-antimonopole pairs in the strong disorder limit. Unfortunately, we are not able to monopoles exactly locate but to obtain a rough position, since they merge in the stringful soup. The integral in Eq. (44) converges very slowly as the counters are close to the singularity string (or points). The integral step is equivalent to the rate of the adiabatic process, which has to be less than the typical energy spacing $2(t + v_i^{max})/N$. When approaching the singularity, the energy gap becomes very small, so the process rate has to be smaller to have convergent results. Therefore, it is very difficult to locate the monopole position if they are in the stringful soup.

The appearance of the antimonopoles in the strong disorder limit is very appealing. It contributes to the polarization in the opposite way that a monopole does. The polarization comes from the charge transportation through the whole sample from one end to the other. Therefore, Eq. (45) for the antimonopole must be highly α dependent shown in the Fig. 13(a). The peak value of $\Delta P(\alpha)$ happens at $\alpha = 0$. After integrating over α by Eq. (46), we obtained $\Delta P = -1.0$. This result indicates that the antimonopole may be located at $\alpha = 0$. In Fig. 13(b), we found that the energy gap closes at $\alpha = 0$, supporting this observation. In Figs. 13(c) and 13(d), we show the energy gap at $\alpha = 0$ along Q_1 and Q_2 directions, respectively. In fact, the structure of the antimonopole is highly anisotropic. The energy gap has a valleylike structure at $\alpha = 0$. Figure 13(e) shows the energy gap along the valley. The slope of the energy gap function along the valley is roughly ten times smaller than other directions. In other words, the antimonopole looks like a football more than a round ball. This anisotropy can be understood in terms of the resonance tunneling, as we will see in the next section.
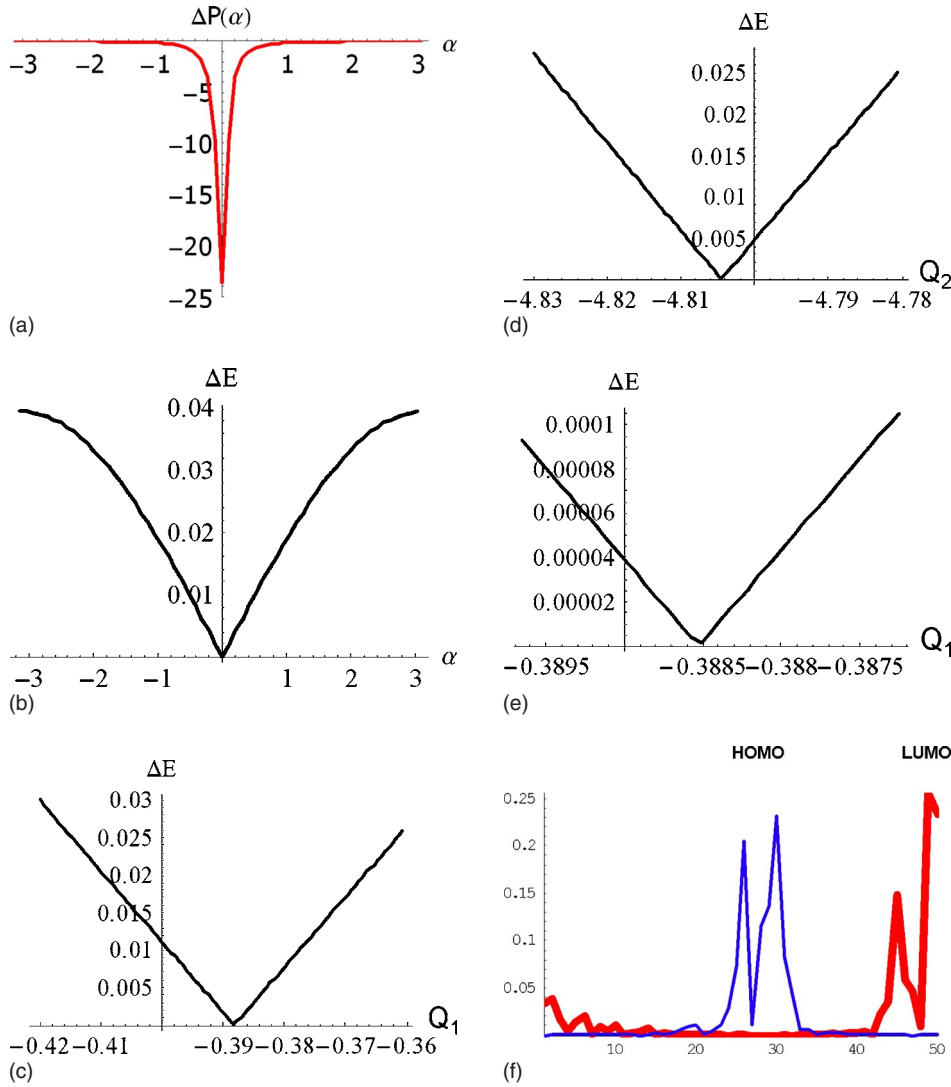
FIG. 13. (Color online) Some properties of antimonopole. (a) the α dependence of Eq. (45) around the antimonopole. (b)–(d) The energy gap functions of the antimonopole along the α, Q_1, and Q_2 directions. (d) The gap function along the valley. The antimonopole is not spherically symmetric. The gap function at $\alpha=0$ has a deep valley because the slopes along the valley is ten times smaller than other directions. (f) The wave functions of the HOMO and LUMO at the antimonopole. In (b)–(e), the axes are in the unit of t_{nn}.

Another quantity to measure the extendedness of a state is the Thouless number defined by

$$\mathcal{N}_T = \frac{E(\alpha=\pi) - E(\alpha=0)}{\delta E}, \tag{47}$$

where $E(\alpha)$ is the energy of the state and δE is the typical energy spacing. We plot the Thouless number of the HOMO in Fig. 14. We found a ridge distribution that coincides with the valley in the energy gap function. The antimonopole is located at the ridge but is not necessarily the highest one. The Thouless number at the ridge is one order of magnitude larger than the other points in the vicinity in the parameter space. It suggests that the high boundary condition sensitivity must dominate the physics at the antimonopole. It leads to the resonance tunneling in the Anderson insulator.[33]

C. Resonance tunneling

We now compare the numerical results with the picture of resonance tunneling discussed in Sec. III B. In the resonance-tunneling scenario, we can deal with the periodic system by identifying x_3 with x_1. It leads to $k_3 = k_1$. In such a

periodic system, as is apart from an open system, E_F is no longer a tunable parameter, but corresponds to discrete energy levels of the system. Thus, S_i, α_i, and β_i are smooth functions of Q_1, Q_2, and an energy E. Because the periodic system is threaded by a flux of $\alpha\Phi_0$, we require that
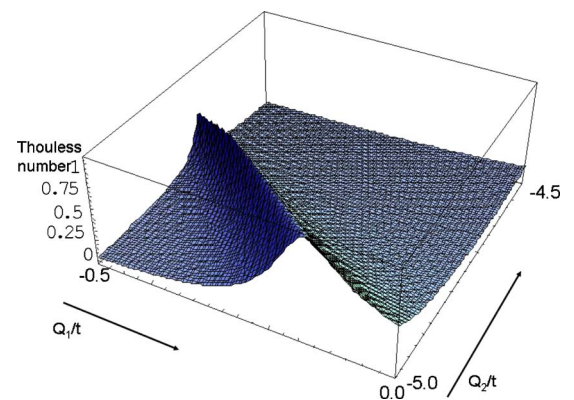

FIG. 14. (Color online) The Thouless number in the vicinity of the antimonopole. The Thouless number has a ridge structure which exactly coincides with the valley in the gap function.
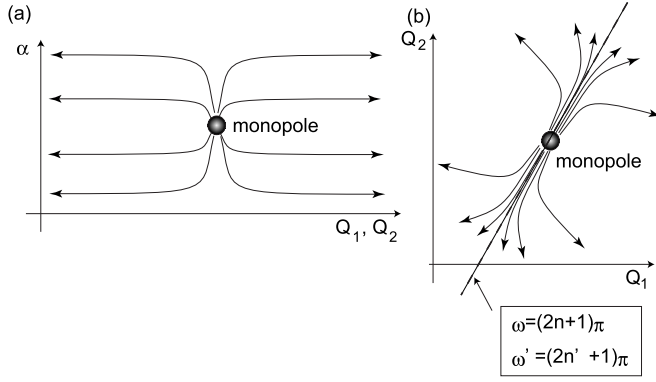
FIG. 15. Distribution of the vector field $\vec{F}$ around the monopole. (a) The field $\vec{F}$ is mostly uniform in the α direction because $\xi \ll L$, except for the vicinity of the monopole. (b) The field is anisotropic in the $Q_1 - Q_2$ plane.

$$\Theta \begin{pmatrix} A_3 \\ B_3 \end{pmatrix} = \begin{pmatrix} A_1 \\ B_1 \end{pmatrix} = e^{i\alpha} \begin{pmatrix} A_3 \\ B_3 \end{pmatrix}. \tag{48}$$

It yields $\det(\Theta - e^{i\alpha}) = 0$, i.e., Re $\theta_{11} = \cos \alpha$. Because θ_{11} is a function of Q_1, Q_2, and E, this defines an (discrete) energy level of the system as a function of Q_1 and Q_2.

We study the monopoles in the framework of resonance tunneling. As the monopoles appear at band-crossing points, we have to look for degenerate solutions of Eq. (48). Namely, we look for cases with two (degenerate) states for fixed Q_1, Q_2 and E. This happens if and only if the matrix Θ is equal to $e^{i\alpha}$. This condition reduces to

$$S_1 = S_2, \tag{49}$$

$$\omega \cong 2 \int_{x_1''}^{x_2'} k(x)dx = (2n+1)\pi, \tag{50}$$

$$\omega' \cong 2 \int_{x_2''}^{x_3} k(x)dx + 2 \int_{x_1}^{x_1'} k(x)dx = (2n'+1)\pi, \tag{51}$$

$$\alpha = -(n+n'+1)\pi, \tag{52}$$

where n and n' are integers. Because S_1, S_2, and ω and ω' are functions of Q_1, Q_2, and E, the three conditions (49)–(51) determine a set of isolated points in the $Q_1 - Q_2 - E$ space. Combining with Eq. (52), we get isolated points in the $Q_1 - Q_2 - \alpha$ space, corresponding to the monopoles/antimonopoles.[38] Except for the vicinity of the monopoles/antimonopoles, the field $\vec{F}$ is almost α independent because the system is almost intact with the change of α. Thus, the distribution of the field $\vec{F}$ is as shown in Fig. 15(a). In contrast to a small-sized model $\xi \sim L$ in Ref. 38, in our disordered model ($\xi \ll L$) the "near-field" region where the flux density is α dependent is limited only in the very close vicinity of the monopoles/antimonopoles.

Equations (50) and (51) are the Bohr quantization conditions, meaning that there are two localized states around x_2 and x_3 ($\equiv x_1$) having the same energy. In general, when there

are two localized states with the same energy, displacing each other by a high potential peak, there is a small tunneling matrix element between them. It gives a small energy splitting between bonding and antibonding states. As a result, the degeneracy is lifted. Nevertheless, when equality (49) holds, it guarantees that the hybridization between them cancels exactly, and the degeneracy is not lifted even after one takes the tunneling into account. Thus, the two localized states are in resonance with each other. Equation (52) means that such exact degeneracy occurs only when α is equal to π or 0, confirming our numerical result.

If we change Q_1 and Q_2 to make $S_1 \neq S_2$ with conditions (50) and (51) preserved, there occurs a small splitting [$\sim O(e^{-2S_i})$] to the otherwise degenerate states due to a small unbalance between S_1 and S_2. Conditions (50) and (51) specify one direction in the $Q_1 - Q_2$ plane from the monopole. Along this direction, the gap remains nonzero but very small, thereby the field $\vec{F}$ becomes large, as schematically shown in Fig. 15(b). In our numerical results, this direction corresponds to the valley direction in the energy gap, and the ridge in the Thouless number in Fig. 14. Thus, the anisotropy of the energy gap in the $Q_1 - Q_2$ plane is of the order $e^{2S_i} \sim e^{L/\xi}$. Because in our numerical calculation $L = 50$ and $\xi \sim 7$, the anisotropy of the monopole is $e^{2S_i} \sim e^{L/\xi} \sim e^7 \sim 10^3$, which should be compared with the numerical value ~ 10 in the previous subsection. Their difference can be attributed to finiteness of the mesh size in the numerical calculation; the mesh may not be fine enough to reproduce the anisotropy $\sim 10^3$. We also note that the strings observed in the numerical calculation can be regarded as the curve of $\omega = (2n+1)\pi$ and $\omega' = (2n'+1)\pi$, with S_1 and S_2 unrestricted.

D. Discussion

In Fig. 13(f), we show the wave functions of the HOMO and LUMO, which support the resonance tunneling scheme. At the resonance, the energy of HOMO and LUMO are degenerate. If HOMO sits at x_1, LUMO can be viewed as the resonance state at the potential valley x_2. Therefore, by means of LUMO, HOMO can tunnel through the whole sample. We must emphasize that this mechanism is topological as that in the pure case.

The adiabatic rate depends on the energy gap. At the resonance, the wave functions of the HOMO and the LUMO do not overlap. By tuning the parameters, the overlapping integral between these two states are not zero, and thus the gap opens up. Again, the rates at which the gap opens with the parameters are not necessarily the same. Therefore, the monopole (antimonopole) structure is not necessarily isotropic. In fact, it can be highly anisotropic, as shown in our calculation. Then, the adiabatic rate is restricted by the minimal gap along the contour. It can be roughly estimated as e^{-L/ξ_R}, where ξ_R is the localization length at the resonance.

The current results for the periodic/twisted boundary condition is consistent with those for the open boundary condition. The topological structure in the open boundary condition, namely, the vortices, can be regarded as a projection of the monopoles to a two-dimensional plane. The anisotropic flux distribution and the anisotropic phase gradient are two

facets of the resonance tunneling. While the results for the open boundary condition is more applicable to the real materials and design, the nontrivial generation of the monopole-antimonopole shown in the periodic/twisted boundary condition case illustrates the deep topological structure in the strong disordered systems.

V. CONCLUSION

In this paper, we have studied the charge pumping and dielectric response in a disordered insulator for both the open boundary condition and periodic/twisted boundary condition. As for the open system coupled to the leads, we have found the quantum mechanically enhanced dielectric response in nanoscopic/mesoscopic disordered insulators, which give a guide for fast and low-dissipation ferroelectric thin films of the FeRAM. The phase of the reflection coefficient r is a key parameter for pumping and has the rich structure in the parameter plane. The topological nature of the insulator dictates the phase winding of r around the vortex where $r=0$ and $|t|=1$. In a pure insulator, this corresponds to the gapless point. In the disordered case, it corresponds to the resonance tunneling through the sample, whose position varies with the chemical potential.

With the periodic closed system, we can consider the three dimensional parameter space $\vec{Q}=(Q_1,Q_2,\alpha)$, where Q_1 is the site energy alternation, Q_2 is the bond dimerization, and α is the phase twist for the boundary condition. In this three-dimensional space, one can discuss the monopoles and their associated gauge field distribution, which are again interpreted in terms of the resonant tunneling.

The existence of the resonant tunneling in the parameter space is guaranteed by the topological properties of the charge pumping, and only two parameters such as Q_1 and Q_2 need to be tuned to realize it. These parameters can be controlled experimentally by the external electric field and pressure. Therefore, the present theory offers a way to design the enhanced dielectric response in realistic systems by controlling the disorder.

*chern@issp.u-tokyo.ac.jp

[1] R. Resta, Rev. Mod. Phys. **66**, 899 (1994).

[2] R. M. Martin, Phys. Rev. B **9**, 1998 (1974).

[3] R. Resta, Ferroelectrics **136**, 51 (1992).

[4] R. D. King-Smith and D. Vanderbilt, Phys. Rev. B **47**, 1651 (1993).

[5] G. Ortiz and R. M. Martin, Phys. Rev. B **49**, 14202 (1994).

[6] S. Onoda, S. Murakami, and N. Nagaosa, Phys. Rev. Lett. **93**, 167602 (2004).

[7] S. Murakami, S. Onoda, and N. Nagaosa (unpublished).

[8] D. J. Thouless, Phys. Rev. B **27**, 6083 (1983).

[9] Q. Niu and D. J. Thouless, J. Phys. A **17**, 2453 (1984).

[10] S. Onoda, C.-H. Chern, S. Murakami, Y. Ogimoto, and N. Nagaosa, Phys. Rev. Lett. **97**, 266807 (2006).

[11] T. Egami, S. Ishihara, and M. Tashiki, Science **261**, 1307 (1993).

[12] N. Nagaosa, J. Phys. Soc. Jpn. **55**, 2754 (1986).

[13] P. Monceau, F. Y. Nad, and S. Brazovskii, Phys. Rev. Lett. **86**, 4080 (2001).

[14] J. F. Scott, *Ferroelectric Memories* (Springer, New York 2000).

[15] P. A. Lee and T. V. Ramakrishnan, Rev. Mod. Phys. **57**, 287 (1985).

[16] L. E. Cross, Ferroelectrics **76**, 241 (1987).

[17] Q. M. Zhang, V. Bharti, and X. Zhao, Science **280**, 2101 (1998).

[18] S. Horiuchi, R. Kumai, Y. Okimoto, and Y. Tokura, Phys. Rev. Lett. **85**, 5210 (2000).

[19] G. Gruner, Rev. Mod. Phys. **60**, 1129 (1988).

[20] M. Switkes, C. M. Marcus, K. Campman, and A. G. Gossard, Science **283**, 1907 (1999).

[21] Y. Levinson, O. Entin-Wohlman, and P. Wolfre, Physica A **302**, 335 (2001).

[22] O. Entin-Wohlman and A. Aharony, Phys. Rev. B **66**, 035329 (2002).

[23] V. Kashcheyevs, A. Aharony, and O. Entin-Wohlman, Phys. Rev. B **69**, 195301 (2004).

[24] S. Datta, *Electronic Transport in Mesoscopic Systems* (Cambridge University Press, Cambridge, 1995).

[25] A. Aharony, O. Entin-Wohlman, and Y. Imry, J. Phys. Soc. Jpn. **72**, 112 (2002).

[26] P. W. Brouwer, Phys. Rev. B **58**, R10135 (1998).

[27] M. Büttiker and A. Prêtre, Z. Phys. B: Condens. Matter **94**, 133 (1994).

[28] J. E. Avron, A. Elgart, G. M. Graf, and L. Sadun, J. Stat. Phys. **116**, 425 (2004).

[29] P. W. Anderson, Phys. Rev. **109**, 1492 (1958).

[30] F. J. Wegner, Z. Phys. B **25**, 327 (1976).

[31] E. Abrahams, P. W. Anderson, D. C. Licciardello, and T. V. Ramakrishnan, Phys. Rev. Lett. **42**, 673 (1979).

[32] A. MacKinnon and B. Kramer, Phys. Rev. Lett. **47**, 1546 (1981).

[33] M. Y. Azbel, Phys. Rev. B **28**, 4106 (1983).

[34] W.-K. Shih and Q. Niu, Phys. Rev. B **50**, 11902 (1994).

[35] F. S. Galasso, in *International Series of Monographs in Solid State Physics* (Oxford University Press, New York, 1970), Vol. 7.

[36] S. Asanuma, M. Fukunaga, Y. Uesu, R. Haumont, B. Dkhil, C. Malibert, and J.-M. Kiat, Jpn. J. Appl. Phys., Part 1, part 1 **43**, 6581 (2004).

[37] A. Zee, Phys. Lett. **135B**, 307 (1984).

[38] D. Cohen, Phys. Rev. B **68**, 155303 (2003).